Published in final edited form as:

Mol Cancer Res. 2018 November ; 16(11): 1687–1700. doi:10.1158/1541-7786.MCR-17-0526.

CD38 Inhibits Prostate Cancer Metabolism and Proliferation by Reducing Cellular NAD+ Pools

Jeffrey P. Chmielewski[1], **Sarah C. Bowlby**[1], **Frances B. Wheeler**[1], **Lihong Shi**[1], **Guangchao Sui**[1], **Amanda L. Davis**[1], **Timothy D. Howard**[4], **Ralph B. D'Agostino Jr.**[2,3], **Lance D. Miller**[1,2], **S. Joseph Sirintrapun**[6], **Scott D. Cramer**[5], and **Steven J. Kridel**[1,2]

[1]-Department of Cancer Biology, Wake Forest School of Medicine, Winston-Salem, North Carolina,

[2]-Comprehensive Cancer Center at Wake Forest Baptist Medical Center, Winston-Salem, North Carolina,

[3]-Public Health Sciences-Department of Biostatistical Sciences, Wake Forest School of Medicine, Winston-Salem, North Carolina,

[4]-Department of Biochemistry, Wake Forest School of Medicine, Winston-Salem, North Carolina,

[5]-Department of Pharmacology, University of Colorado Denver, Aurora, Colorado,

[6]-Department of Pathology, Memorial Sloan Kettering Cancer Center, New York, New York.

Abstract

Tumor cells require increased rates of cell metabolism to generate the macromolecules necessary to sustain proliferation. They rely heavily on nicotinamide adenine dinucleotide (NAD^+) as a cofactor for multiple metabolic enzymes in anabolic and catabolic reactions. NAD^+ also serves as a substrate for poly ADP-ribose polymerases (PARPs), sirtuins, and cyclic ADP-ribose synthases. Dysregulation of the cyclic ADP-ribose synthase CD38, the main NAD'ase in cells, is reported in multiple cancer types. This study demonstrates a novel connection between CD38, modulation of NAD^+, and tumor cell metabolism in prostate cancer (PCa). CD38 expression inversely correlates with PCa progression. Expressing CD38 in PCa cells lowered intracellular NAD^+, resulting in cell cycle arrest and expression of $p21^{Cip1}$ (CDKNA1). In parallel, CD38 diminishes glycolytic and mitochondrial metabolism, activates AMP-activated protein kinase (AMPK), and inhibits fatty acid and lipid synthesis. Pharmacological inhibition of nicotinamide phosphoribosyltransferase

Corresponding Author: Steven J. Kridel, Wake Forest School of Medicine, 1 Medical Center Blvd. Winston-Salem, NC 27157, (336) 716-7299, skridel@wakehealth.edu.

Authors' Contribution

- Conception and Design: J. Chmielewski, S. Kridel
- Development of Methodology: J. Chmielewski, S. Kridel
- Acquisition of data: J. Chmielewski, S. Kridel, L. Miller, S. Cramer, L. Shi, J. Sirintrapun, T. Howard, F. Wheeler, A. Davis, Bowlby, S.
- Analysis and Interpretation of data: J. Chmielewski, S. Kridel, R. D'Agostino Jr., L. Miller, J. Sirintrapun
- Writing, review, and/or revision of the manuscript: J. Chmielewski, S. Kridel

Conflict of Interest Disclosure Statement: The authors declare no potential conflicts of interest.

(NAMPT) mimicked the metabolic consequences of CD38 expression, demonstrating similarity between CD38 expression and NAMPT inhibition. Modulation of NAD^+ by CD38 also induces significant differential expression of the transcriptome, producing a gene expression signature indicative of a non-proliferative phenotype. Altogether, in the context of prostate cancer, the data establish a novel role for the CD38-NAD^+ axis in the regulation of cell metabolism and development.

Keywords

Prostate cancer; CD38; NAMPT; Metabolism; NAD(H); lipid; glycolysis; mitochondria

Introduction

Nicotinamide adenine dinucleotide (NAD^+) metabolism is associated with everything from aging and healthy lifespan, to diabetes, neurocognitive function, and cancer, among others (1,2). NAD^+ connects to cellular metabolism in various ways. First, it is a necessary cofactor for multiple anabolic and catabolic reactions, in doing so providing a crucial link to energy production and macromolecular synthesis (3). For example, NAD^+ is reduced to NADH during glycolysis and the TCA cycle, producing an electron carrier for subsequent adenosine triphosphate (ATP) generation. Conversely, the phosphorylated form, NADPH, is a cofactor for fatty acid synthesis. Because deregulated cellular metabolism is an established hallmark of oncogenic transformation, it is reasonable to assume NAD^+ metabolism must be regulated accordingly (4).

There are multiple pathways by which NAD^+ can be synthesized, and they can be segregated into either the *de novo* or salvage pathways. Most tissues and oncogenic cells synthesize NAD^+ via the salvage pathway (5). The salvage pathway is a two-step reaction that recycles nicotinamide into NAD^+ and is catalyzed by nicotinamide phosphoribosyltransferase (NAMPT). NAD^+ turnover in cancer cells is dramatically increased relative to non-proliferating healthy cells, making NAD^+ metabolism an attractive therapeutic target (6). NAD^+ levels can also be modulated by enzymatic consumption. There are three classes of enzymes that consume NAD^+: the poly-ADP ribose polymerases (PARPs), sirtuins, and cyclic ADP-ribose synthases (7–9). While PARPs and sirtuins have multiple roles in cancer biology, including response to DNA damaging reagents and modulation of protein modification, among others, CD38 is the primary NAD'ase in mammalian cells (10). CD38 is a cyclic ADP-ribose synthase that localizes to the cell membrane and elsewhere throughout the cell including the endoplasmic reticulum (ER), golgi, and mitochondria (11,12). CD38 hydrolyzes NAD^+ to produce ADP-ribose (ADPR), which is covalently attached to proteins to modify their function (9). Alterations in CD38 expression occur in a variety of cancers including hematological malignancies, glioma, pancreatic cancer, and prostate cancer (PCa) (13–15). Decreased expression of CD38 in prostate luminal cells is sufficient to drive PCa and is linked to lower overall survival (16). Conversely, *CD38* expression in higher in pancreatic cancer compared to normal tissue (17). Although expression of CD38 is linked to disease progression, the metabolic consequences of CD38 expression in PCa have not been defined.

We previously demonstrated that NAMPT activity is required to support fatty acid and lipid synthesis in PCa (18). Therefore, we hypothesized that CD38, through its NAD'ase activity, also regulates energy production and lipid synthesis in PCa. The data presented herein demonstrate that CD38 expression is reduced in PCa and that expressing CD38 in PCa cells affects multiple metabolic processes to reprogram cells in favor of a non-proliferative state. Collectively, our data suggest that loss of CD38 is a key event in oncogenic transformation in prostate that confers a metabolic advantage to tumor cells, thus providing new insight into the mechanisms underlying tumor cell metabolism.

Materials and Methods

Materials

Antibodies for acetyl-CoA carboxylase 1 (ACC1), phospho-ACC1 (S79), AMPK, phospho-AMPK (T172), Sirt1, and Sirt3 (C73E3) were obtained from Cell Signaling Technologies (Beverly, MA, USA), antibodies against CD38 and FOXO1 were from Abcam (Cambridge, MA, USA), antibodies for SLC22A3 and β-Actin were purchased from Sigma-Aldrich (St. Louis, MO, USA) and antibody for Ac-FOXO1 was purchased from Santa Cruz Biotechnology, Inc. (Dallas, TX, USA). Secondary antibodies for goat-anti-mouse and goat-anti-rabbit were purchased from BioRad (Hercules, CA, USA). The NAMPT inhibitor FK866 was obtained from Cayman Chemical Company (Ann Arbor, MI, USA). Nicotinamide adenine dinucleotide (NAD^+), nicotinamide mononucleotide (NMN), doxycycline hyclate, and puromycin dihydrochloride were purchased from Sigma-Aldrich (St. Louis, MO, USA). ^{14}C-Acetate was purchased from PerkinElmer (Boston, MA, USA) and ^{14}C – Choline from American Radiolabeled Chemicals (St. Louis, MO, USA). Retinoic acid (all-*trans*-Retinoic acid; ATRA) and 5-Azacytidine (Aza) were obtained from Sigma-Aldrich (St. Louis, MO, USA). All primers for qPCR were purchased from Integrated DNA Technologies (San Jose, CA, USA).

Cell Culture, drug treatments, and transfection

LNCaP, PC-3, and DU145 cell lines were obtained from the American Type Culture Collection (ATCC, Manassas, VA, USA). Normal prostate epithelial cells (PRECs) were obtained from Lonza (Switzerland). Cells were routinely subjected to *mycoplasma* testing. PCa cell lines were cultured in RPMI 1640 (Gibco) supplemented with 10% fetal bovine serum (FBS), Penicillin (100 units/ml), and Streptomycin (100 μg/mL) at 37°C and 5% CO_2. PRECs were cultured in Clonetics™ prostate cell growth medium as directed by the manufacturer. Cell lines and clones were used over 10–20 passages following thawing. FK866 was dissolved in DMSO and used at the concentrations and times as indicated. Vehicle control cells were treated with DMSO (0.01%). NMN (500μM) and NAD^+ (100μM) were dissolved in sterile water and cotreated with FK866 at the time of administration.

For transfection, cells were cultured in complete RPMI 1640 and 10% FBS without antibiotics for 48Hrs prior to seeding. After seeding, cells were transfected with varying amounts (500ng-2μg) of plasmid DNA containing either the CD38 cDNA under the direction of a doxycycline inducible promoter or the same vector without CD38. Cells were transfected using Lipofectamine LTX with Plus Reagent (Thermo Fisher, Waltham, MA

USA). Transfected cells were selected with puromycin (4μg/ml) (Sigma-Aldrich, St. Louis, MO, USA) until individual colonies were formed. Clonal populations were established from single colonies and maintained on puromycin (1μg/ml) to retain selection and CD38 was induced with doxycycline (1μg/ml) for the indicated times.

Immunohistochemistry of CD38 expression

CD38 staining intensity was determined from benign, prostatic intraepithelial neoplasia (PIN), and prostate adenocarcinoma cores from a tissue microarray obtained from BioMax Inc. (Rockville, MD, USA). Slides were deparaffinized and rehydrated by xylene/ethanol wash. Slides were then incubated with antigen unmasking solution in a pressure cooker at 97°C for 30 minutes. Cooled slides were blocked in 1% bovine serum albumin (BSA) in 1x phosphate-buffered saline (PBS) for 10 minutes at room temperature. CD38 antibody was incubated at a 1:1000 dilution in 1% BSA overnight at 4°C. Slides were washed three times with PBS and incubated with horseradish peroxidase (HRP) secondary antibodies, incubated for 10 minutes in 3, 3-diaminobenzidine (DAB) solution, washed three times in 1x PBS, and counterstained with hematoxylin. TMA cores were independently scored by staining intensity ranging from 0 to 3 with 0 representing the lowest intensity.

Western blotting

Cells were treated as indicated for individual experiments, harvested, washed with 1x cold PBS, and lysed in buffer containing 1% Triton X-100, 20mM Tris-HCl (pH 8.3), 5mM EDTA, and protease inhibitors (1μM sodium orthovanadate, 1μM sodium fluoride, 200nM okadaic acid, 5μg/ml aprotinin, pepstatin, and leupeptin, and 200μM PMSF). Protein concentrations for individual samples were assayed using BioRad DC reagents, using BSA as a standard. Samples were resolved via SDS-PAGE, and transferred to nitrocellulose blotting membrane. Membranes were blocked and incubated with primary and secondary antibodies as previously described (18). Enhanced chemiluminescence (Perkin Elmer Life science, Boston, MA, USA) was used to detect immuno reactive bands.

Total NAD^+ quantification

Quantification of total cellular NAD^+ was performed using an EnzyChrom NAD^+/NADH Assay Kit (Hayward, CA, USA) as described previously (18). Briefly, cells were seeded (1.5×10^5 cells/dish) in triplicate in 10cm dishes and treated as indicated. After treatement, cells were harvested by trypsinization, counted, and NAD^+ determined according to manufacturer's instructions. Total NAD^+ levels were normalized to protein from an equivalent number of cells and made relative to vehicle treated cells.

Cell count and viability assays

PCa cells were plated in 6-well plates in triplicate and allowed to adhere for 24Hrs prior to treatment with doxycycline (1μg/ml) or ATRA (Sigma-Aldrich, St. Louis, MO, USA). At the indicated time points, cells were trypsinized, pelleted, and resuspended in a known volume. Cell counts were established using a Countess automated cell counter. Live versus dead cells were quantified by trypan blue exclusion using a Countess automated cell counter. Cell growth was determined by normalizing cell numbers at the indicated time points to the

number of cells plated. Doubling times were determined using relative growth values from T24 and T96 time points.

The viability of cells expressing CD38 treated with FK866 was determined using Cell Titer-Glo 2.0 (Promega, Madison, WI, USA). Briefly, cells treated with vehicle or doxycycline (1μg/mL) were plated in 96-well plates (N=7) and allowed to adhere for 8Hrs prior to the addition of FK866. Luminescence was detected using a FLUOstar Optima spectrometer (BMG Labtech, Cary, NC, USA) and viability was determined relative to control.

Cell Cycle Analysis

PCa cells were treated with doxycycline (1μg/ml) or vehicle for 96Hrs. They were then trypsinized, washed twice in cold PBS, and fixed in cold 70% methanol for 30 minutes at 4°C. Following fixation, cells were washed twice with PBS and treated with RNase A (100μg/ml) for 15 minutes (Thermo Fisher, Waltham, MA, USA) followed by staining with propidium iodide (50μg/ml) (Invitrogen, Carlsbad, CA, USA). Flow cytometry was performed on a Becton Dickinson Accuri C6 analyzer (Franklin Lakes, NJ, USA) and analyzed using FlowJo V10 software (FlowJo, LLC., Ashland, Oregon, USA). The percent of cells in each phase of the cell cycle was determined using the Watson Pragmatic algorithm available in the FlowJo software.

Determination of *CD38* gene methylation status

PCa cells were seeded into 10cm dishes and allowed to adhere overnight before treating with ATRA (1.2μM) or azacytidine (5μM) for 96Hrs (Sigma-Aldrich, St. Louis, MO, USA). They were then trypsinized, washed twice with PBS, and lysed in Qiagen Buffer RLT buffer supplemented with 2-mercaptoethanol (140μM) (Sigma-Aldrich, St. Louis, MO, USA). DNA/RNA purification was performed using an AllPrep DNA/RNA Mini Kit (Qiagen, Germantown, MD, USA). Pyrosequencing assays were designed using PyroMark Assay Design 2.0 (version 2.0.1.15) to sequence two target regions. Region 1 sequenced the genomic region chr4:15,780,321–15,780,394 (Human genome build GRCh37/hg19) and contained 13 CpG sites. Primers for region 1 were as follows: forward, 5’ –TGGGTATTGAGGGGATA GTAG-3’; reverse (biotinylated), 5’-AACCCCAAACTCCCTACTCAACA-3’; sequencing, 5’-TTGAGGGGATAGTAGGGT-3’. Region 2 sequenced genomic region chr4:15,780,514–15,780,586 and contained 6 CpG sites. Primers for region 2 were as follows: forward (biotinylated), 5’-TGGTGTTGAGTAGGGAGT-3’; reverse, 5’-CCAC AAACTTTACAAACCACTTAAATATCC-3’; sequencing, 5’-AAAATAAACTACAAC-3’. Genomic DNA (1μg) from each sample (N=2) was treated with sodium bisulfite using the EZ 96-DNA methylation kit (Zymo Research, CA, USA), following the manufacturer’s standard protocol. Pyrosequencing was performed according to the PyroMarkMD protocol and sequenced with a PyroMark Q96 MD instrument. Methylation analysis was performed with Pyro Q-CpG (version 1.0.9).

Quantitative real time PCR gene expression analysis

PCa cells were seeded into 10cm dishes and treated with either ATRA (1.2μM) or azacytidine (5μM) for 96Hrs (Sigma-Aldrich, St. Louis, MO, USA). LNCaP cells treated

with doxycycline (1μg/ml) for 96Hrs served as positive control. Cells were then harvested, washed twice with PBS, and lysed in Qiagen RLT buffer supplemented with 2-mercaptoethanol (140μM) (Sigma-Aldrich, St. Louis, MO, USA). DNA/RNA purification was performed using an AllPrep DNA/RNA Mini Kit (Qiagen, Germantown, MD, USA). qPCR was performed using a Roche LightCycler II and 1-Step Brilliant SYBR Green qRT-PCR master mix (Agilent Technologies, Santa Clara, CA, USA). Forward and reverse primer sequences for CD38 primer sets 1 and 2 and β-ACTIN were as follows: CD38 Forward 1: 5'-CGCGATGCGTCAAGTACACTGAA-3', CD38 Reverse 1: 5'-CGGTCTGAGTTCCCAACTTCATTAG-3'; CD38 Forward 2 : 5'-GGAGAAAGGACT: GCAGCAACAACC-3', CD38 Reverse 2: 5'- CTGCGGGATCCATTGAGCATCACAT-3'; β-ACTIN Forward : 5'- CGG AGT ACT TGC GCT CAG GA – 3', β-ACTIN Reverse: 5' – CCA CGA AAC TAC CTT CAA CTC CAT CAT G-3'. The Roche LightCycler 489 protocol was: 50°C for 30 Min, 95°C for 10 Min, then a three-step amplification (30 Sec at 95°C, 30 Sec at 55°C, 1 Min at 68°C) x 45 cycles, rest at 4°C. Changes in gene expression were determined using the ΔΔCt method as previously described (19).

Measurement of extracellular acidification rates (ECAR) and oxygen consumption rates (OCR)

PCa cells were pretreated either with vehicle, FK866 (100nM), FK866 + NMN (500μM), or FK866 + NAD^+ (100μM) for 24Hrs or doxycycline 72Hrs prior to plating in 24-well plates and incubated overnight at 37°C (6×10^5 cells/well; XF24 plates, Agilent, Santa Clara, CA, USA). To measure ECAR and OCR, RPMI culture medium was changed to minimal DMEM assay media supplemented with glutamine (2mM) (ECAR) or XF Assay Medium supplemented with glucose (25mM) and sodium pyruvate (1mM) (OCR) followed by a 1Hr incubation at 37°C in the absence of CO_2. Baseline ECAR and OCR were measured on a Seahorse XF24 extracellular flux analyzer (Agilent; Santa Clara, CA, USA). Basal glycolytic and mitochondrial functions were established following injections to final concentrations of glucose (10 mM) or oligomycin (1 μM), respectively. Maximum glycolytic and mitochondrial potential were achieved by injecting to a final concentration of oligomycin (1 μM) or carbonyl cyanide 4-(trifluoromethoxy) phenylhydrazone (FCCP) (0.5 μM), respectively. Glycolytic and mitochondrial inhibition were achieved following injection to a final concentration of 2-Deoxy-D-glucose (100 mM) or combination of rotenone and antimycin A (1 μM each), respectively. All measurements were normalized to cell counts determined at the conclusion of each assay.

Quantification of glucose and lactate levels

PCa cells were plated in 6-well plates in triplicate and allowed to adhere overnight prior to treatment with doxycycline (1μg/ml) for 96Hrs. To determine the amount of glucose consumed or lactate produced the existing culture media was removed, cells were rinsed with PBS, and 1.5mL of fresh RPMI was added. Samples were taken immediately following media change (T0) and after 12Hrs. Glucose and lactate levels were determined using Biovision Glucose and Lactate Assay Kits (Milpitas, CA, USA). Glucose and lactate concentrations were normalized to cellular protein.

Fatty acid and lipid synthesis

Fatty acid and lipid synthesis were determined by incorporation of ^{14}C-acetate or ^{14}C-choline into lipid as previously described (18). Briefly, 5×10^5 cells treated with vehicle or doxycycline (1μg/ml) for 72Hrs were seeded in 24-well plates for 24Hrs (N = 4 wells per treatment). Cells were incubated with ^{14}C-acetate (1μCi) or ^{14}C-choline (1μCi) for 2Hrs. Cells were then harvested, washed with PBS, and lysed in hypotonic buffer (20mM Tris-HCL (pH 7.5), 1mM EDTA, and 1mM DTT). The lipid fraction was extracted using chloroform/methanol (2:1), and incorporation of labeled acetate or choline into newly synthesized lipid was determined by scintillation counting and normalized to cellular protein.

Metabolite Profiling

Metabolomic profiling was conducted on PC3 cells treated with vehicle or FK866 (100nM) for 24Hrs (N = 4). Samples were collected and submitted for analysis as directed by Metabolon, Inc. Onsite sample preparation was carried out using an automated MicroLab STAR© system utilizing a series of proprietary organic and aqueous extractions to remove the protein fraction. Samples were analyzed on gas chromatography/mass spectrometry (GC/MS) and liquid chromatography/tandem mass spectrometry (LC/MS^2) platforms and analyzed against known libraries of purified compounds as previously described (20). Statistical significance for pair-wise comparisons was determined using Welch's t-tests and/or Wilcoxon's rank sum tests. Compound clustering and classification was performed using random forest analyses (21). All statistical modeling was performed using R.

Genomic Analysis

RNASeq analysis was conducted in the Cancer Genomics Shared Resource of Wake Forest Baptist Comprehensive Cancer Center. LNCaP cells transfected with either an empty vector or CD38 expression construct were plated (5×10^5 cells/dish) in 10cm dishes and treated with doxycycline (1μg/ml) for 96Hrs (N = 5 per group). Total RNA was purified from cell lines using the RNeasy Plus Micro Kit (Qiagen, Germantown, MD, USA) with genomic DNA removal. RNA integrity (RIN) was assessed via electrophoretic tracing on an Agilent Bioanalyzer. RNASeq libraries were constructed from samples (RIN>7.0) using an Illumina TruSeq Stranded Total RNA kit with Ribo-Zero Gold rRNA depletion. Libraries were sequenced on an Illumina NextSeq 500 DNA sequencer using 75-nt single end reads generating 45 to 55 million uniquely mapped reads/sample. The quality of raw sequencing reads was evaluated by FASTQC analysis (Babraham Bioinformatics). Read alignment was conducted using the STAR sequence aligner and gene counts established using Feature Counts software (22,23). Differentially expressed genes (DEGs) were verified using the DESeq2 algorithm and statistically significant results defined as $p \leq 0.05$ after adjusting for false discovery (Benjamini-Hochberg) (24).

Gene set enrichment analysis was performed as described by Subramanian et al. (25). Briefly, genes with base mean values below five reads were eliminated from analysis and $\log_2$ fold changes were arranged in descending order. Gene symbols were loaded into GSEA software and run against hallmark gene symbol v6.0 with a false collapsable data set run at 1000 permutations.

CD38 gene expression and methylation status were investigated using the TCGA prostate adenocarcinoma (PRAD) provisional dataset (N = 491) as accessed through the cBioPortal Web Resource (26). Methylation (HM450) beta-values for *CD38* were plotted against *CD38* RNASeq (V2 RSEM) expression values using the cBioPortal query interface (http://www.cbioportal.org/). Pearson and Spearman correlations were used to evaluate the relationship between the two measures.

Survival analysis of SLC22A3 expression as a predictor of biochemical recurrence was performed using GraphPad Prism version 5.00 for Windows (San Diego, CA, USA). Survival and expression data was derived from patient samples from two independent cohorts (27,28). SLC22A3-low expression was defined as values one standard deviation below the mean relative to the remainder (SLC22A3-High). Statistical significance was derived using log rank (Mantel Cox) analysis.

Statistical Analysis

Data were graphically displayed using bar-charts or box-plots to allow groups to be compared visually. Pairwise comparisons were made using unpaired two-tailed t-tests. Groups were compared using one-way analysis of variance (ANOVA) models. If there was evidence of an overall difference among groups (i.e., significant F-test in ANOVA) subsequent pairwise comparisons were made using multiple comparison adjustments Tukey's HSD (honest significant difference) as appropriate to determine which groups differed from each other. For gene expression analysis, a linear contrast was fit in the ANOVA model to examine whether there was a linear relationship in the outcome going across the groups ordered Benign, PIN, PCa, Met-HR. Levels of significance were denoted by three groupings, *$p \leq 0.05$, **$p \leq 0.01$, and ***$p \leq 0.001$, comparisons with p-values between 0.01 and 0.05 considered as marginally significant to account for the multiple comparisons being made, whereas p-values less than 0.01 were considered as significant accounting for multiple comparisons.

Results

CD38 expression is inversely correlated with prostate cancer progression.

In order to understand the role of CD38 in PCa, protein expression was first determined in normal prostate epithelial cells (PREC) and the tumorigenic C4–2, PC3, LNCaP, and DU145 cell lines. PREC's expressed CD38 whereas expression was nearly absent in the tumorigenic lines (Figure 1A). Consistent with CD38 expression and its reported NAD'ase activity, PREC's had lower total NAD^+ levels compared to tumorigenic lines with 2.5 nmole/μg protein, whereas the tumorigenic lines ranged from 5.23–11.8 nmoles/μg protein ($p \leq 0.05$, Figure 1A). It has been demonstrated that low CD38 expression is associated with both biochemical recurrence and metastasis (16). The GEO dataset GSE6099 was used to determine if *CD38* expression is decreased with PCa progression (29). ANOVA suggested a highly significant group effect between benign, prostatic interepithelial neoplasia (PIN), PCa, and metastatic hormone refractory (Met-HR) disease states ($F = 23.5$, $p \leq 0.001$) (Figure 1B). Pairwise comparisons revealed benign samples had significantly higher *CD38* expression relative to each of the other stages ($p \leq 0.001$). Furthermore, expression of *CD38*

in PIN margins was greater relative to both PCa ($p \leq 0.05$) and Met-HR ($p \leq 0.019$). There was no difference between PCa and Met-HR. Linear contrast analysis (1 degree of freedom) of the trend in expression across all four groups was found to be highly significant ($F = 54.33$, $p \leq 0.001$) (Figure 1B). CD38 protein expression was also determined by immunohistochemistry (IHC). ANOVA followed by post-hoc Student-Newman-Keuls analysis demonstrated a 24% reduction of CD38 staining intensity in benign vs. PIN, 36% decrease in PIN vs PCa, and a 50% decrease in benign vs PCa ($p \leq 0.001$, Figure 1C). Overall these results indicate loss of CD38 expression during PCa progression occurs in a stepwise manner and is correlated with elevated NAD^+ levels.

Expression of CD38 reduces total NAD^+ levels and inhibits cell proliferation.

To determine if CD38 acts as a NAD'ase in PCa, total NAD^+ levels were determined following CD38 induction. Induction of CD38 in DU145, LNCaP, and PC3 cells was confirmed by western blot and was sufficient to reduce total NAD^+ levels in DU145 cells by 31%, in LNCaP cells by 29%, and in PC3 cells by 91% relative to vehicle ($p \leq 0.05$, Figure 2A). DU145 empty vector cells treated with doxycycline showed no significant change in total NAD^+ (Figure 2A). These data support the notion that CD38 can alter NAD^+ levels between normal and cancer cells. Sirtuins require NAD^+ for their catalytic activity and FOXO1 is one SIRT1 substrate whose activity is regulated by acetylation and affected by changes in NAD^+ levels (30). Therefore, we next determined the impact of CD38 on FOXO1 acetylation. Expression of CD38 increased FOXO1 acetylation 3.4-fold, similar to what was observed following treatment with sirtinol (Figure 2B) or the NAMPT inhibitor FK866 (Figure 2B). The effect on acetylation was independent of CD38-induced change in Sirt1 and 3 expression (Figure 2C). The impact of CD38 expression on cell proliferation was determined by trypan blue exclusion in all three cell lines. CD38 induced a significant proliferation blockade at multiple time points with the most significant effects occurring in DU145 (34%, $p \leq 0.01$), LNCaP (32%, $p \leq 0.001$), and PC3 (21%, $p \leq 0.001$) cells at 96Hrs post induction, without increasing dead cells. This demonstrates that CD38 is sufficient to inhibit proliferation by limiting NAD^+ (Figures 2D, G, and J). Decreased cell numbers were accompanied by a small but significant G_0/G_1 blockade and subsequent reduction of cells in S and G_2/M (Figures 2E, H, and K). Moreover, CD38 expression increased the doubling time of DU145 cells from 44 hrs to 55.6 hrs, of LNCaP cells from 36 hrs to 44.5 hrs, and of PC3 cells from 44 hrs to 59.8 hrs ($p < 0.01$) (Figures 2F, I, and L). Although CD38 reduced proliferation, cells expressing CD38 remained sensitive to NAMPT inhibition by FK866, as has been previously demonstrated in pancreatic cancer (17). Treatment of CD38 expressing cells with 2.5, 5, and 10 nM FK866 further reduced viability by 17%, 36%, and 39% respectively ($p \leq 0.01$, Figure 2M). These data reveal the requirement for NAD^+ by PCa cells.

CD38 expression is induced by ATRA.

There is a retinoic acid response element (RARE) in the *CD38* promoter and RA can induce CD38 expression in some cells (31,32). PCa cells were treated with all-trans retinoic acid (ATRA) to see if CD38 expression can be induced and overcome silencing. Treatment with ATRA was sufficient to induce expression of CD38 in three PCa cell lines, although there was no dose effect over the range tested (Figure 3A). ATRA also reduced total NAD^+ in

LNCaP and DU145 cells ($p \leq 0.01$), which correlated with a significant decrease in cell number ($p \leq 0.01$, Figure 3B-C). These data provide another demonstration of the connection between CD38 and NAD^+ in PCa. The presences of CpG islands spanning exon 1 and intron 1 of the *CD38* gene can be methylated (33,34). The Cancer Genome Atlas (TCGA) prostate adenocarcinoma (PRAD) provisional data set also demonstrated that there is a significant inverse correlation between *CD38* expression and *CD38* methylation (Pearson R = −0.667, Spearman = −0.826) suggesting that *CD38* may be subject to negative regulation by methylation in PCa (Figure 3D). LNCaP and PC3 cells were treated with ATRA and azacytidine to determine their impact on the methylation status of 19 potential methylation sites (Figure 3E and G). While there is some difference in the overall methylation status of *CD38* amongst these sites, ATRA did not impact the methylation status of either site, despite significant *CD38* expression in LNCaP and PC-3 cells ($p \leq 0.001$, Figure 3F and H). On the other hand, azacytidine reduced the overall methylation of *CD38* in PC3 ($p \leq 0.05$) but not LNCaP cells while increasing *CD38* expression in both cell lines ($p \leq 0.001$, Figure 3F and H). These data suggest that ATRA can induce CD38 expression, although not through changes in the CpG sites analyzed here. They also suggest that methylation is a mechanism that contributes to decreased CD38 expression in PCa.

CD38 reduces glycolytic and mitochondrial capacity.

The role of CD38 in regulating cellular metabolism was determined at several levels. The effect of CD38 on glycolysis was determined by Seahorse analysis. Figure 4A illustrates the influence of CD38 on the extracellular acidification rate (ECAR) of DU145 cells. Quantification of the ECAR demonstrates that CD38 reduced basal glycolysis and glycolytic capacity by 32% and 44%, respectively ($p \leq 0.05$, Figure 4B). Similarly, CD38 in PC3 cells reduced basal glycolysis by 27% and glycolytic capacity by 30% ($p \leq 0.05$, Figure 4C). CD38 did not affect either basal glycolysis or glycolytic capacity in LNCaP cells (Figure 3D). Mitochondrial stress assays were performed to determine the effect of CD38 expression on cellular oxygen consumption rates (OCR). Figure 4E illustrates the influence of CD38 on the OCR of LNCaP cells. When quantified, basal respiration was reduced by 24% ($p \leq 0.05$), maximal respiration by 45% ($p \leq 0.01$), and spare respiratory capacity by 25% ($p \leq 0.05$) (Figure 4F). In PC3 cells, CD38 reduced basal respiration by 43% ($p \leq 0.001$) maximal respiration by 39% ($p \leq 0.01$), and spare respiratory capacity by 27% ($p \leq 0.05$) (Figure 4G). In DU145 cells, CD38 reduced basal OCR by 36% ($p \leq 0.05$), maximal respiration by 39% ($p \leq 0.05$), and spare respiratory capacity by 35% ($p \leq 0.05$) (Figure 4H). In accordance with decreased ECAR, CD38 reduced glucose consumption from 14.3 to 7.1 μM/μg protein and 15.2 to 8.1 μM/μg protein in DU145 and PC3 cells, respectively ($p \leq 0.001$, Figure 4I and J). A concomitant decrease in lactate production from 23.2 to 18.4 μM/μg protein in DU145 cells ($p \leq 0.001$) and 25.3 to 16 μM/μg protein in PC3 cells ($p < 0.001$) accompanied decreased glucose consumption (Figure 4I and J). These data provide novel insight into metabolic regulation by CD38 and suggest CD38 silencing is required for full metabolic capacity in PCa cells.

Pharmacological inhibition of NAMPT reduces glycolytic and mitochondrial capacity.

Because CD38 expression may mimic inhibition of NAD^+ synthesis, the metabolic consequences of NAMPT inhibition were determined. Figure 5A illustrates the impact of

NAMPT inhibition by FK866 on the ECAR of PC3 cells. NAMPT inhibition reduced basal glycolysis and glycolytic capacity by 30% and 49%, respectively ($p \leq 0.001$, Figure 5B), both of which were fully restored with exogenous NMN or NAD^+. Similar results were observed in DU145 cells where basal glycolysis was reduced by 29% ($p \leq 0.05$) and glycolytic capacity by 40% ($p \leq 0.05$) (Figure 5C). Similar to the effects of CD38 on ECAR, there were no observed differences in LNCaP cells following NAMPT inhibition (Figure 5D). We next determined the consequence of NAMPT inhibition on OCR in PC3 cells (Figure 5E). Maximal respiration and spare respiratory capacity were reduced by 37% ($p \leq 0.01$) and 35% ($p \leq 0.01$), respectively (Figure 5F). Supplementation of NMN and NAD^+ rescued the effect of FK866. DU145 cells had a more pronounced reduction in maximal respiration and spare respiratory capacity, being reduced by 54% ($p \leq 0.01$) and 56% ($p \leq 0.01$), respectively (Figure 5G). No changes in either measurement were detected in LNCaP cells (Figure 5H).

To compliment glycolytic and mitochondrial flux assays, metabolite levels were measured following NAMPT inhibition in PC3 cells (Figure 5I-K). As expected, treatment with FK866 reduced the NAD^+ metabolites nicotinamide, NAD^+, NADH, and $NADP^+$ by 87%, 86%, 71%, and 95% relative to vehicle, respectively ($p \leq 0.001$, Figure 5I). Metabolites involved in glycolysis upstream of glyceraldehyde phosphate dehydrogenase (GAPDH), the reaction in glycolysis that utilizes NAD^+ as a cofactor, were increased. Specifically, glucose, glucose-6-phosphate, and sorbitol were increased by 56%, 91%, and 35% relative to vehicle, respectively ($p \leq 0.05$, Figure 5J). Lactate, the byproduct of glycolysis, was decreased by 14% ($p \leq 0.05$, Figure 5J). Metabolites in the tricarboxylic acid (TCA) cycle, which contains multiple enzymes that utilize NAD^+ as a cofactor, were also affected. Citrate and succinate were reduced to 77% ($p \leq 0.05$) and 36% ($p \leq 0.001$) of vehicle (Figure 5K). Fumarate and malate, metabolites upstream of malate dehydrogenase, an NAD^+ dependent enzyme, were increased 207% ($p \leq 0.001$) and 218% ($p \leq 0.001$) relative to vehicle (Figure 5K). These data directly align with the effects of CD38 on glycolytic and mitochondrial metabolism, providing additional evidence to the importance of NAD^+ balance, and that CD38 expression closely mimics NAMPT inhibition.

Expression of CD38 Activates AMPK and Inhibits Fatty Acid and Lipid Synthesis.

We previously reported that NAMPT inhibition activates AMP-activated protein kinase (AMPK) and subsequently inactivates acetyl-CoA carboxylase 1 (ACC1), resulting in decreased fatty acid and lipid synthesis (18). Similarly, CD38 increased the pAMPK/AMPK ratio in PC3, DU145 and LNCaP cells by 1.86-fold, 3.95-fold, and 1.79-fold, respectively (Figure 6A). Consistent with AMPK activation, the ratio of pACC to total ACC in PC3, DU145 and LNCaP cells increased by 2.39-fold, 10.85-fold, and 1.94-fold, respectively. There was little change in FASN levels (Figure 6A). In line with inactivation of ACC1, incorporation of ^{14}C-acetate into fatty acid was reduced by 34% in PC3 cells, 20% in DU145 cells, and by 48% in LNCaP cells ($p \leq 0.01$, Figure 6B). Expression of CD38 had similar effects on the incorporation of ^{14}C-choline into the lipid fraction. Lipid synthesis was reduced by 35%, 32%, and 26% in PC3, DU145 and LNCaP cells, respectively ($p \leq 0.01$, Figure 6C). Taken together, these results indicate that CD38 impedes energy

production and substrate flow, resulting in activation of AMPK and the subsequent inhibition of fatty acid and lipid synthesis.

CD38 reprograms the transcriptome of prostate cancer cells.

To better understand the global impact of CD38 on LNCaP cells, RNASeq was used to determine the extent to which it altered gene expression and biological processes. Of the 34,000 genes analyzed, 14,409 (41%) genes had significant differential expression following induction of CD38 ($p \leq 0.05$, FDR-adjusted). The data were further gated to include only transcripts with a $\log_2$ fold-change of $1 \leq x \leq -1$, revealing 1082 (3.1%) up-regulated and 828 (2.4%) down-regulated genes (data not shown). Gene set enrichment analysis was performed to define molecular signatures consistent with the RNASeq expression profile (Figure 7 A-C). Consistent with the effects of CD38 on proliferation, multiple pathways associated with reduced proliferation were affected by CD38 expression. Among them, the E2F targets (q-value ≤ 0.0001) were the most significant (Figure 7A). As an example, *CDKN1A* expression was increased 2.85-fold by CD38 expression, consistent with a non-proliferative phenotype. Similar to what has been reported in pancreatic cancer, CD38 expression caused an increase in $p21^{Cip1}$ protein expression of 1.53-fold, 6.0-fold, and 1.96-fold in PC3, DU145, and LNCaP cells, respectively, following CD38 expression. Other pathways, including Notch signaling (q-value = 0.005), and G2M checkpoint (q-value ≤ 0.0001), were also highly correlated as signatures that exhibited decreased expression following induction of CD38 (Figures 7B-C). As each pathway carries an important role in cell proliferation, these data establish a connection between expression of CD38 and a reprogramming of the transcriptome in favor of a non-proliferative phenotype. Although the metabolic consequences of CD38 expression in PCa were broad, it appears that the effects are primarily attributed to changes in cellular NAD^+ and not decreases in metabolic gene expression. In general, the relative gene expression levels of enzymes involved in glycolysis, the TCA cycle, fatty acid synthesis, and the electron transport chain (ETC) were below the 2-fold cut off despite multiple transcripts achieving statistical significance (Table 1). It is important to note that of the glycolytic enzymes, there was no change in glyceraldehyde phosphate dehydrogenase *(GAPDH)*, the only enzyme in glycolysis that requires NAD^+. Similarly, expression levels of genes encoding TCA cycle enzymes were similarly unaltered, with the greatest changes occuring in pyruvate dehydrogenase kinase *(PDK1)* (1.49-fold), aconitase 1 *(ACO2)* (1.5-fold), and isocitrate dehydrogenase 1 *(IDH1)* (1.5-fold). These data provide further evidence that decreased mitochondrial output is not the result of decreased gene expression but rather limited availability of NAD^+ to facilitate enzymatic activity. The single greatest change of any metabolic gene occurred in *FASN*, which was reduced 1.92-fold ($p \leq 0.0001$, FDR-adjusted), although there was no detectable change in protein levels. In addition to gene set enrichment analysis, the most differentially expressed gene in the data set was selected for analysis. *SLC22A3* expression increased more than 300-fold (Figure 7D). SLC22A3 protein expression was also increased in LNCaP cells following induction of CD38 and NAMPT inhibition (Figure 7D). Interestingly, the single nucleotide polymorphism (SNP) rs936455 in *SLC22A3* is the single most highly correlated SNP with PCa (35). *SLC22A3* is also one of the most significantly down-regulated genes in high-Gleason grade tumors (29). Therefore, the correlation between biochemical recurrence and *SLC22A3* expression was determined in the Taylor and Yu cohorts which contain 181

primary and 37 metastases or 66 primary and 83 normal (adjacent or donor) samples, respectively (27,28). Consistent with the inverse association between *SLC22A3* and high-Gleason grade tumors, high *SLC22A3* was associated with increased time to biochemical recurrence in the Taylor and Yu cohorts (Figure 7E). These data establish a novel connection between CD38 and cellular processes, aside from metabolism, that regulate proliferation and are associated with PCa progression.

Discussion

Tumor cells require an available pool of NAD^+ for appropriate metabolic control and post-translational protein modification, among other functions, to support survival and proliferation. Intracellular NAD^+ levels can be modulated by increased synthesis, in particular through the salvage pathway, where NAMPT is the rate limiting enzyme. In fact, NAMPT expression is increased in several cancers, partially illustrating the importance of NAD^+ in tumor biology (36). One of the principle roles of NAD^+ is as a cofactor in metabolic reactions, serving to support hydride transfer reactions. While these reactions affect whether NAD^+ is oxidized or reduced, they do not consume or alter NAD^+ levels. CD38 is the primary NAD'ase in mammalian cells (10). Here we demonstrate that CD38 expression is decreased in PCa and regulates the metabolic potential of PCa cells. This provides a mechanistic explanation for why loss of CD38 in prostate luminal progenitor cells results in PCa, particularly in response to inflammation (16).

Although we and others have demonstrated that CD38 expression is reduced in PCa, the mechanism by which CD38 expression is decreased is unknown. The *CD38* gene is located on chromosome 4p15.32; a region not frequently lost in PCa (37). Using the TCGA prostate adenocarcinoma (PRAD) provisional data set, we establish a strong negative correlation between *CD38* methylation and expression. This suggests that epigenetics could be a determinant of CD38 expression in PCa. Interestingly, *CD38* has CpG islands that span exon 1 and intron 1 that may be potential epigenetic regulatory sites (34). Moreover, *CD38* also has a retinoic acid response element (RARE) in its promoter region (33). The data demonstrate that ATRA is sufficient to induce CD38 expression, but not through the CpG sites tested. Similarly, azacytidine can induce CD38 expression, although likely through other CpG sites as well since expression in LNCaP was independent of changes in the examined sites. Overall, the data suggest that strategies to induce CD38 expression could be one mechanism to decrease NAD^+ in PCa and perhaps affect therapeutic response and hint that there are epigenetic or other elements in *CD38* that regulate its expression.

The data also demonstrate a direct link between CD38 and metabolic capacity in PCa. Expression of CD38 reduced the glycolytic and mitochondrial potential of PCa cell lines reflected by decreases in ECAR and OCR. This is in line with decreased NAD^+ levels and reduced proliferation. Interestingly, decreased CD38 expression in PCa is opposite of that in aging where CD38 expression increases with age (38). On the other hand, in both cases CD38 regulates mitochondrial metabolism. It is worth noting that, while CD38 reduced the OCR in LNCaP cells, there was no observed effect on ECAR. Moreover, LNCaP cells rely less on glycolysis and more on mitochondrial metabolism, so the metabolic impact of CD38 is most likely primarily through mitochondrial metabolism. These findings are in line with

previous reports, including ours, that some cells are resistant to NAMPT inhibition; perhaps indicating that NAD^+ can exist in distinct pools in some cells (18,39,40). Thus, we posit that CD38 targets mitochondrial NAD^+ pools in all lines tested. It appears that most of the metabolic consequences of CD38 expression are due to diminished total NAD^+ rather than changes in expression as the majority of metabolic enzymes showed no change at the mRNA level following CD38 expression. However, it does not rule out the enzymes being affected by acetylation as CD38 induces acetylation of the Sirt1 substrate FOXO1 and also affects the acetylation status of P53 (41). Because sirtuins can regulate metabolic processes including ATP production, anti-oxidative stress response, lipid synthesis, and the metabolic switch to anaerobic glycolysis (42,43) we posit that CD38 impacts cellular metabolism through acetylation and depleted metabolite flow by limiting available NAD^+.

PCa has a lipogenic phenotype indicated by high expression of lipogenic enzymes and increased uptake of metabolic tracers of lipogenesis (44). We previously reported the link between NAD^+ synthesis and lipogenesis in PCa (18). In line with this, CD38 expression induced AMPK activation and subsequent phosphorylation of the canonical AMPK substrate ACC1. Accordingly, CD38 reduced fatty acid and lipid synthesis, suggesting that reduced CD38 expression is required in some part to support the lipogenic phenotype associated with PCa. Interestingly, CD38 does not have a significant impact on ACC1 or FASN expression, suggesting that CD38 regulates bioenergetics and substrate flow through the pathway, but that oncogenic drivers control enzyme expression. It is noteworthy that CD38 expression in PCa mimics the metabolic consequences of NAMPT inhibition, as assessed by OCR, ECAR, and lipid synthesis, suggesting that alterations in NAD^+ levels, regardless of the cause, yield similar results.

Although CD38 clearly affects cellular metabolism, it also impacts pathways that control proliferation, including Notch signaling, E2F targets, and G2M checkpoint. Notch signaling has both pro and anti-proliferative potential in PCa and is linked to metastatic disease (45,46). Interestingly, Notch signaling can be triggered by Sirt1 activation and modulated in response to variations in NAMPT expression (47). Additionally, activated NOTCH is a known repressor of $p21^{Cip1}$ expression in PCa (48). Therefore, it is reasonable that CD38 expression suppressed NOTCH signaling and increased $p21^{Cip1}$ expression in the E2F signaling hallmark. In addition to indicators of reduced proliferation, CD38 also affects *SLC22A3* expression. Decreased SLC22A3 expression is associated with tumor progression and poor patient survival in a variety of solid tumors including ovarian, pancreatic, and PCa (49,50). Moreover, *SLC22A3* is among the most down-regulated genes in high-Gleason grade PCa (29,51). Our data demonstrate a correlation between SLC22A3 and recurrence free survival, and the same is also true for CD38 (16), suggesting a correlation between the two genes in PCa. Silencing of *SLC22A3* in prostate is regulated by genetic polymorphisms in the proximal promoter and aberrant methylation of the promoter region (52). In PCa cell lines, the *SLC22A3* promoter is variably methylated, with LNCaP cells being less methylated than in DU145 and PC3 cells (52). This may explain why CD38 and FK866 induce SLC22A3 in LNCaP cells but not PC3 and DU145 cells. These data provide the first demonstration that changes in NAD^+ metabolism can regulate SLC22A3.

Collectively, the data illustrate a novel connection between CD38, modulation of NAD^+, and PCa tumor cell metabolism. We propose a model in which silencing of CD38 elevates NAD^+ bioavailability and reprograms prostate cells in favor of macromolecule biosynthesis and a pro-proliferative phenotype. The finding that low CD38 expression in luminal progenitor cells is sufficient to initiate PCa (16), combined with our metabolic and gene expression data, provides a critical connection between CD38, NAD^+ metabolism, and PCa progression.

Acknowledgments

Grant Support

- This research was supported by 5R01CA16503 (SJK) and 5T32Hl091797–10 (JPC). Research reported in this publication was supported by the National Cancer Institute's Cancer Center Support Grant award number P30CA012197 issued to the Wake Forest Baptist Comprehensive Cancer Center. The content is solely the responsibility of the authors and does not necessarily represent the official views of the National Cancer Institute.

Citations

1. Chiarugi A, Dolle C, Felici R, Ziegler M. The NAD metabolome--a key determinant of cancer cell biology. Nat Rev Cancer 2012;12:741–52 [PubMed: 23018234]
2. Verdin E NAD(+) in aging, metabolism, and neurodegeneration. Science 2015;350:1208–13 [PubMed: 26785480]
3. Di Stefano M, Conforti L. Diversification of NAD biological role : the importance of location. Febs Journal 2013;280:4711–28 [PubMed: 23848828]
4. Hanahan D, Weinberg RA. Hallmarks of cancer: the next generation. Cell 2011;144:646–74 [PubMed: 21376230]
5. Kennedy BE, Sharif T, Martell E, Dai C, Kim Y, Lee PWK, et al. NAD(+) salvage pathway in cancer metabolism and therapy. Pharmacological Research 2016;114:274–83 [PubMed: 27816507]
6. Hasmann M, Schemainda I. FK866, a highly specific noncompetitive inhibitor of nicotinamide phosphoribosyltransferase, represents a novel mechanism for induction of tumor cell apoptosis. Cancer Res 2003;63:7436–42 [PubMed: 14612543]
7. Li XL, Kazgan N. Mammalian Sirtuins and Energy Metabolism. International Journal of Biological Sciences 2011;7:575–87 [PubMed: 21614150]
8. Jagtap P, Szabo C. Poly(ADP-ribose) polymerase and the therapeutic effects of its inhibitors. Nature Reviews Drug Discovery 2005;4:421–40 [PubMed: 15864271]
9. Lee HC. Structure and enzymatic functions of human CD38. Molecular Medicine 2006;12:317–23 [PubMed: 17380198]
10. Aksoy P, White TA, Thompson M, Chini EN. Regulation of intracellular levels of NAD: A novel role for CD38. Biochemical and Biophysical Research Communications 2006;345:1386–92 [PubMed: 16730329]
11. Shrimp JH, Hu J, Dong M, Wang BS, MacDonald R, Jiang H, et al. Revealing CD38 Cellular Localization Using a Cell Permeable, Mechanism-Based Fluorescent Small-Molecule Probe. Journal of the American Chemical Society 2014;136:5656–63 [PubMed: 24660829]
12. Liang M, Chini EN, Cheng J, Dousa TP. Synthesis of NAADP and cADPR in Mitochondria. Archives of Biochemistry and Biophysics 1999;371:317–25 [PubMed: 10545220]
13. Kramer G, Steiner G, Fodinger D, Fiebiger E, Rappersberger C, Binder S, et al. High Expression of a CD38-Like Molecule in Normal Prostatic Epithelium and its Differential Loss in Benign and Malignant Disease. The Journal of Urology 1995;154:1636–41 [PubMed: 7563309]
14. Liu AY, Roudier MP, True LD. Heterogeneity in Primary and Metastatic Prostate Cancer as Defined by Cell Surface CD Profile. The American Journal of Pathology 2004;165:1543–56 [PubMed: 15509525]

15. Zhao YJ, Graeff R, Lee HC. Roles of cADPR and NAADP in pancreatic cells. Acta Biochimica Et Biophysica Sinica 2012;44:719–29 [PubMed: 22677461]
16. Liu X, Grogan TR, Hieronymus H, Hashimoto T, Mottahedeh J, Cheng DH, et al. Low CD38 Identifies Progenitor-like Inflammation-Associated Luminal Cells that Can Initiate Human Prostate Cancer and Predict Poor Outcome. Cell Reports 2016;17:2596–606 [PubMed: 27926864]
17. Chini CCS, Guerrico AMG, Nin V, Camacho-Pereira J, Escande C, Barbosa MT, et al. Targeting of NAD Metabolism in Pancreatic Cancer Cells: Potential Novel Therapy for Pancreatic Tumors. Clinical Cancer Research 2014;20:120–30 [PubMed: 24025713]
18. Bowlby SC, Thomas MJ, D'Agostino RB, Kridel SJ. Nicotinamide Phosphoribosyl Transferase (Nampt) Is Required for De Novo Lipogenesis in Tumor Cells. Plos One 2012;7:12
19. Schmittgen TD, Livak KJ. Analyzing real-time PCR data by the comparative C-T method. Nature Protocols 2008;3:1101–8 [PubMed: 18546601]
20. DeHaven CD, Evans AM, Dai HP, Lawton KA. Organization of GC/MS and LC/MS metabolomics data into chemical libraries. Journal of Cheminformatics 2010;2:12
21. Breiman L Random Forests. Machine Learning 2001;45:5–32
22. Dobin A, Davis CA, Schlesinger F, Drenkow J, Zaleski C, Jha S, et al. STAR: ultra fast universal RNA-seq aligner. Bioinformatic 2012;29:15–21
23. Liao Y, Smyth G, Shi W. featureCounts: an efficient general purpose progarm for assigning sequence rease to genomic features. Bioinformatics 2014;30:923–30 [PubMed: 24227677]
24. Love M, Huber W, Anders S. Moderated estimation of fold change and dispersion for RNA-seq data with DESeq2. Genome Biology 2014;12:550
25. Subramanian A, Tamayo P, Mootha VK, Mukherjee S, Ebert BL, Gillette MA, et al. Gene set enrichment analysis: a knowledge-based approach for interpreting genome-wide expression profiles. Proc Natl Acad Sci U S A 2005;102:15545–50 [PubMed: 16199517]
26. Gao J, Aksoy BA, Dogrusoz U, Dresdner G, Gross B, Sumer SO, et al. Integrative analysis of complex cancer genomics and clinical profiles using the cBioPortal. Sci Signal 2013;6:pl1 [PubMed: 23550210]
27. Taylor BS, Schultz N, Hieronymus H, Gopalan A, Xiao Y, Carver BS, et al. Integrative genomic profiling of human prostate cancer. Cancer Cell 2010;18:11–22 [PubMed: 20579941]
28. Yu YP, Landsittel D, Jing L, Nelson J, Ren B, Liu L, et al. Gene expression alterations in prostate cancer predicting tumor aggression and preceding development of malignancy. J Clin Oncol 2004;22:2790–9 [PubMed: 15254046]
29. Tomlins SA, Mehra R, Rhodes DR, Cao X, Wang L, Dhanasekaran SM, et al. Integrative molecular concept modleing of prostate cancer progression. nature genetics 2016;49:41–51
30. Liu HY, Xing R, Cheng XF, Li QR, Liu F, Ye H, et al. De-novo NAD(+) synthesis regulates SIRT1-FOXO1 apoptotic pathway in response to NQO1 substrates in lung cancer cells. Oncotarget 2016;7:62503–19 [PubMed: 27566573]
31. Kishimoto H, Hoshino S, Ohori M, Kontani K, Nishina H, Suzawa M, et al. Molecular mechanism of human CD38 gene expression by retinoic acid - Identification of retinoic acid response element in the first intron. Journal of Biological Chemistry 1998;273:15429–34 [PubMed: 9624127]
32. Uruno A, Noguchi N, Matsuda K, Nata K, Yoshikawa T, Chikamatsu Y, et al. All-trans retinoic acid and a novel synthetic retinoid tamibarotene (Am80) differentially regulate CD38 expression in human leukemia HL-60 cells: possible involvement of protein kinase C-δ. Journal of Leukocyte Biology 2011;90:235–47 [PubMed: 21393419]
33. Ferrero E, Saccucci F, Malavasi F. The human CD38 gene: polymorphism, CpG island, and linkage to the CD157 (BST-1) gene. Immunogenetics 1999;49:597–604 [PubMed: 10369916]
34. Nata K, Takamura T, Karasawa T, Kumagai T, Hashioka W, Tohgo A, et al. Human gene encoding CD38 (ADP-ribosyl cyclase/cyclic ADP-ribose hydrolase): Organization, nucleotide sequence and alternative splicing. Gene 1997;186:285–92 [PubMed: 9074508]
35. Eeles RA, Kote-Jarai Z, Giles GG, Al Olama AA, Guy M, Jugurnauth SK, et al. Multiple newly identified loci associated with prostate cancer susceptibility. Nature Genetics 2008;40:316–21 [PubMed: 18264097]
36. Garten A, Petzold S, Korner A, Imai S, Kiess W. Nampt: linking NAD biology, metabolism and cancer. Trends Endocrinol Metab 2009;20:130–8 [PubMed: 19109034]

37. Robinson D, Van Allen Eliezer M, Wu Y-M, Schultz N, Lonigro Robert J, Mosquera J-M, et al. Integrative Clinical Genomics of Advanced Prostate Cancer. Cell;161:1215–28
38. Camacho-Pereira J, Tarrago MG, Chini CCS, Nin V, Escande C, Warner GM, et al. CD38 Dictates Age-Related NAD Decline and Mitochondrial Dysfunction through an SIRT3-Dependent Mechanism. Cell Metabolism 2016;23:1127–39 [PubMed: 27304511]
39. Tolstikov V, Nikolayev A, Dong S, Zhao G, Kuo MS. Metabolomics Analysis of Metabolic Effects of Nicotinamide Phosphoribosyltransferase (NAMPT) Inhibition on Human Cancer Cells. Plos One 2014;9:24
40. Stein LR, Imai S. The dynamic regulation of NAD metabolism in mitochondria. Trends in Endocrinology and Metabolism 2012;23:420–8 [PubMed: 22819213]
41. Aksoy P, Escande C, White TA, Thompson M, Soares S, Benech JC, et al. Regulation of SIRT 1 mediated NAD dependent deacetylation: A novel role for the multifunctional enzyme CD38. Biochemical and Biophysical Research Communications 2006;349:353–9 [PubMed: 16935261]
42. Haigis MC, Sinclair DA. Mammalian Sirtuins: Biological Insights and Disease Relevance Annual Review of Pathology-Mechanisms of Disease. Palo Alto: Annual Reviews; 2010 p 253–95.
43. Hallows WC, Lee S, Denu JM. Sirtuins deacetylate and activate mammalian acetyl-CoA synthetases. Proceedings of the National Academy of Sciences of the United States of America 2006;103:10230–5 [PubMed: 16790548]
44. Liu QP, Luo Q, Halim A, Song GB. Targeting lipid metabolism of cancer cells: A promising therapeutic strategy for cancer. Cancer Letters 2017;401:39–45 [PubMed: 28527945]
45. Su Q, Xin L. Notch signaling in prostate cancer: refining a therapeutic opportunity. Histol Histopathol 2016;31:149–57 [PubMed: 26521657]
46. Bin Hafeez B, Adhami VM, Asim M, Siddiqui IA, Bhat KM, Zhong W, et al. Targeted knockdown of Notch1 inhibits invasion of human prostate cancer cells concomitant with inhibition of matrix metalloproteinase-9 and urokinase plasminogen activator. Clin Cancer Res 2009;15:452–9 [PubMed: 19147749]
47. Wang P, Du H, Zhou CC, Song J, Liu X, Cao X, et al. Intracellular NAMPT-NAD+-SIRT1 cascade improves post-ischaemic vascular repair by modulating Notch signalling in endothelial progenitors. Cardiovasc Res 2014;104:477–88 [PubMed: 25341895]
48. Lefort K, Ostano GP, Mello-Grand M, Calpini V, Scatolini M, Farsetti A, et al. Dual tumor suppressing and promoting function of Notch1 signaling in human prostate cancer. Oncotarget 2016;7:48011–26 [PubMed: 27384993]
49. Mohelnikova-Duchonova B, Strouhal O, Hughes DJ, Holcatova I, Oliverius M, Kala Z, et al. SLC22A3 polymorphisms do not modify pancreatic cancer risk, but may influence overall patient survival. Scientific Reports 2017;7:11 [PubMed: 28127060]
50. Heise M, Lautem A, Knapstein J, Schattenberg JM, Hoppe-Lotichius M, Foltys D, et al. Downregulation of organic cation transporters OCT1 (SLC22A1) and OCT3 (SLC22A3) in human hepatocellular carcinoma and their prognostic significance. Bmc Cancer 2012;12:10 [PubMed: 22233382]
51. True L, Coleman I, Hawley S, Huang CY, Gifford D, Coleman R, et al. A molecular correlate to the Gleason grading system for prostate adenocarcinoma. Proceedings of the National Academy of Sciences of the United States of America 2006;103:10991–6 [PubMed: 16829574]
52. Chen L, Hong C, Chen EC, Yee SW, Xu L, Almof EU, et al. Genetic and epigenetic regulation of the organic cation transporter 3, SLC22A3. Pharmacogenomics Journal 2013;13:110–20 [PubMed: 22231567]

Implications

This research establishes a mechanistic connection between CD38 and metabolic control. It also provides the foundation for the translation of agents that modulate NAD+ levels in cancer cells as therapeutics.

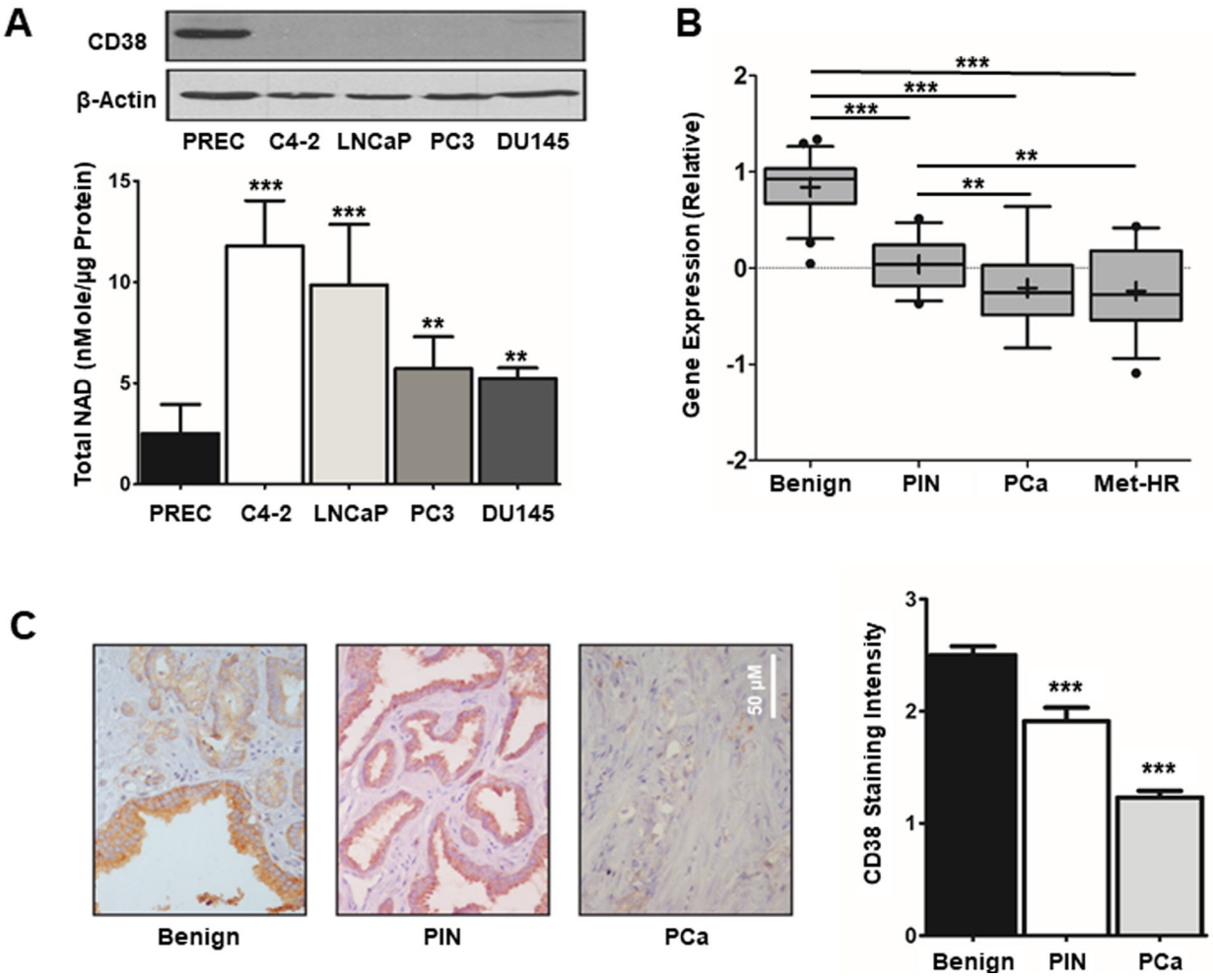

Figure 1: CD38 expression is inversely correlated with prostate cancer progression.

A, CD38 protein expression was determined by western blot in PREC and PCa cells. Colorimetric determination of total NAD^+ levels in PREC and PCa cell lines (N = 3). B, Quantification of relative *CD38* expression from patient samples contained in GEO database GSE6099 containing benign (N = 22), PIN (N = 13), PCa (N = 29), and Met-HR (N = 17) samples (29). C, CD38 expression was determined by immunohistochemistry (IHC) on a tissue microarray containing benign (N = 37), PIN (N = 17), and PCa (N = 37). Staining intensity was independently scored on scale of 0–3. (*$p \leq 0.05$, **$p \leq 0.01$, ***$p \leq 0.001$)

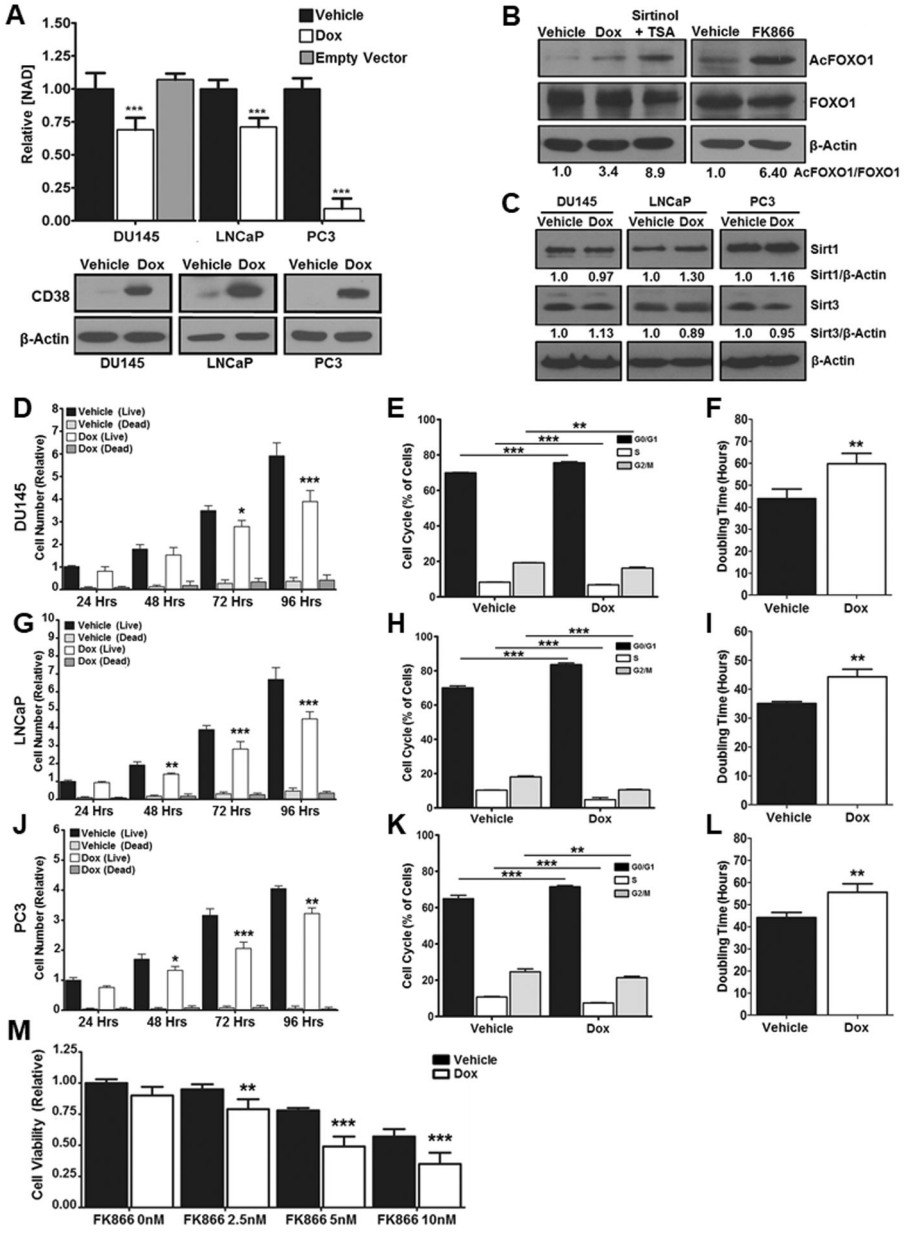

Figure 2: CD38 reduces total NAD$^+$ and inhibits cell proliferation.

A, Total NAD$^+$ levels were measured in PCa cells following treatment with vehicle (dH_2O) or doxycycline (1μg/ml) for 96Hrs (N = 3). Expression of CD38 and β-Actin in PCa cells determined by western blot following 96Hr treatment with doxycycline (1μg/ml). B, Expression of acetylated-FOXO1, total FOXO1, and β-Actin in PC3 cells determined by western blot in response to CD38 expression or treatment with FK866 (100nM). Treatment with Sirtinol (100μM) and Trichostatin A (500μM) for 18Hrs served as positive control. The ratio of acetylated/total FOXO1 was determined by densitometry of single bands using β-Actin as a loading control. C, Expression of Sirt1, Sirt3, and β-Actin in PCa cells was determined by western blot following 96Hr treatment with doxycycline (1μg/ml). Changes in Sirt1 or Sirt3 expression were determined by densitometry of single bands using β-Actin

as a loading control. D, G, and J, Relative cell counts of live and dead PCa cells determined by trypan blue exclusion of cells treated with doxycycline (1μg/ml) for the indicated times (N = 3). E, H, and K, Cell cycle analysis of PCa cells treated with doxycycline (1μg/ml) for 96Hrs. Signal intensity of incorporated propidium iodide corresponding to DNA content was used to gate cells into G0/G1, S, and G2/M phases (N=3). F, I, and L, Doubling time of PCa cells from following 96Hr treatment with doxycycline (1μg/ml) (N=3). M, Viability of DU145 cells treated with doxycycline (1μg/ml) for 72Hrs followed by 24Hr treatment with FK866 at the indicated concentration (N=3). (*$p \leq 0.05$, **$p \leq 0.01$, ***$p \leq 0.001$)

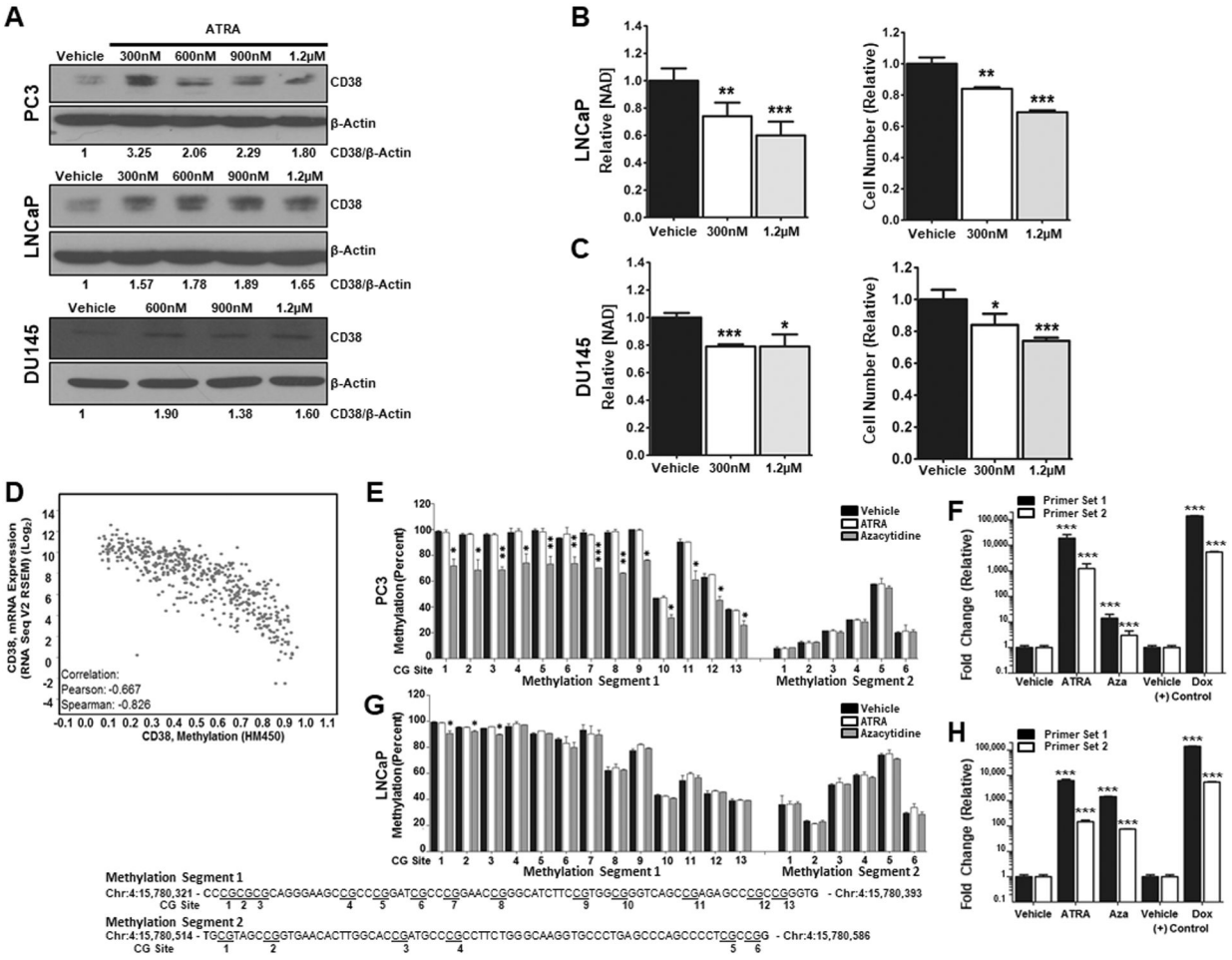

Figure 3: CD38 expression is induced by ATRA.

A, Expression of CD38 following 96Hr treatment with ATRA at the indicated concentration. B-C, NAD^+ levels and cell counts in LNCaP and DU145 cells treated for with ATRA for 96Hrs (N=3). D, *CD38* expression as a function of methylation status determined using data from the TCGA prostate adenocarcinoma (PRAD) provisional data set (N = 491). E & G, Pyrosequencing data from PC3 and LNCaP cells representing the percent of methylated CG sites in two segments of intron 1 of the *CD38* gene following 96Hr treatment with ATRA (1.2μM) or azacytidine (5μM) (N=2). F & H, Fold change in CD38 mRNA in response to treatment with ATRA (1.2μM) or azacytidine (5μM) for 96Hrs. (*p ≤ 0.05, **p ≤ 0.01, ***p ≤ 0.001)

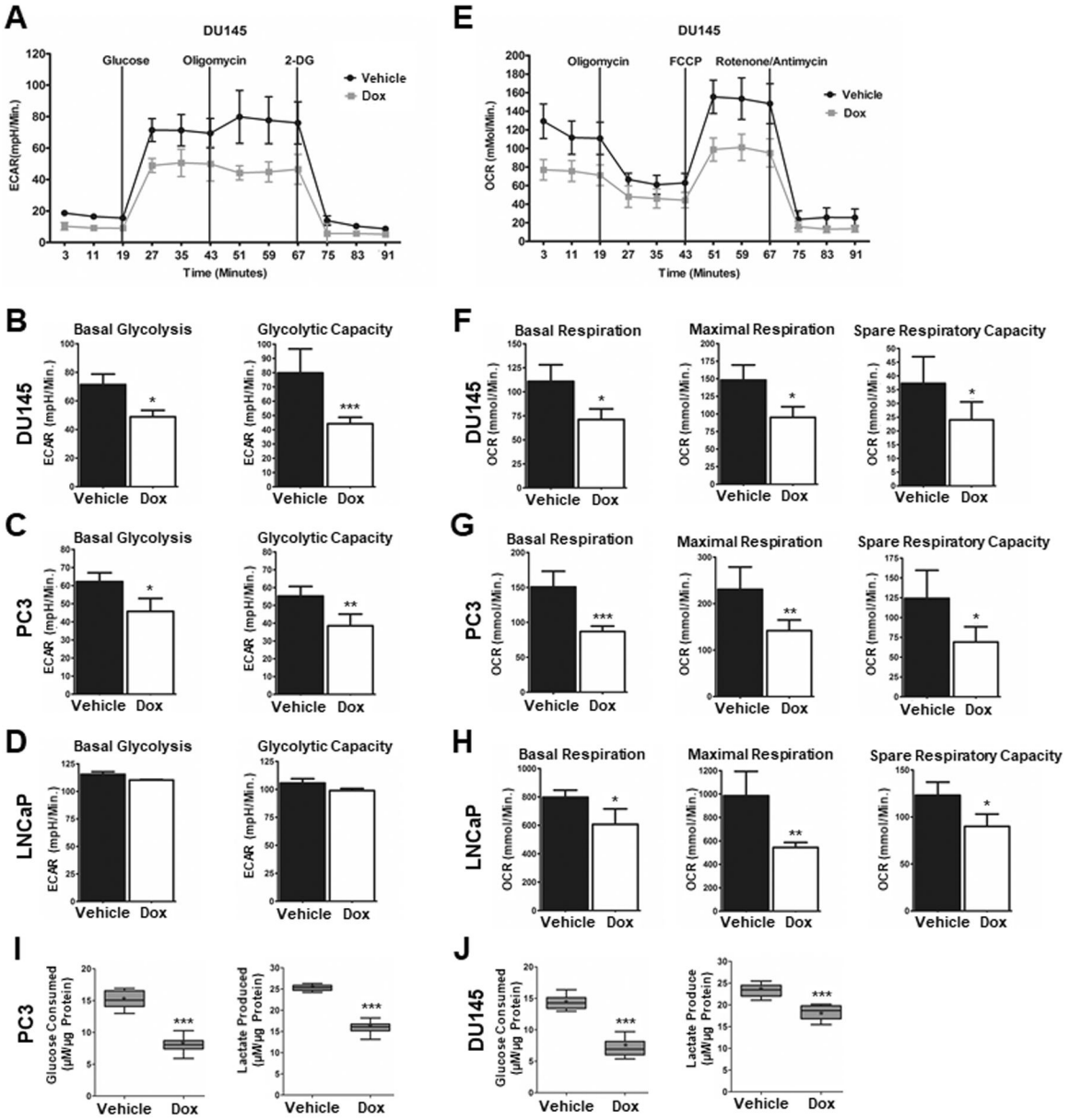

Figure 4: CD38 reduces glycolytic and mitochondrial capacity.

A, Representative trace of a glycolytic stress test in DU145 cells following treatment with doxycycline (1μg/ml) for 96Hrs to induce CD38 (N = 3). B-D, Quantification of basal glycolysis and glycolytic capacity in DU145, PC3, and LNCaP cells treated with doxycycline (1μg/ml) for 96Hrs (N = 3). E, Representative trace of a mitochondrial stress test in DU145 cells following treatment with doxycycline (1μg/ml) for 96Hrs (N = 3). F-H, Quantification of basal respiration, maximal respiration, and spare respiratory capacity in DU145, PC3, and LNCaP cells treated with vehicle (dH_2O) or doxycycline (1μg/ml) for 96Hrs (N = 3). I-J, Quantification of glucose consumed or lactate produced in PC3 and DU145 cells following 96Hr treatment with doxycycline (1μg/ml) (N=6). (*$p \leq 0.05$, **$p \leq 0.01$, ***$p \leq 0.001$)

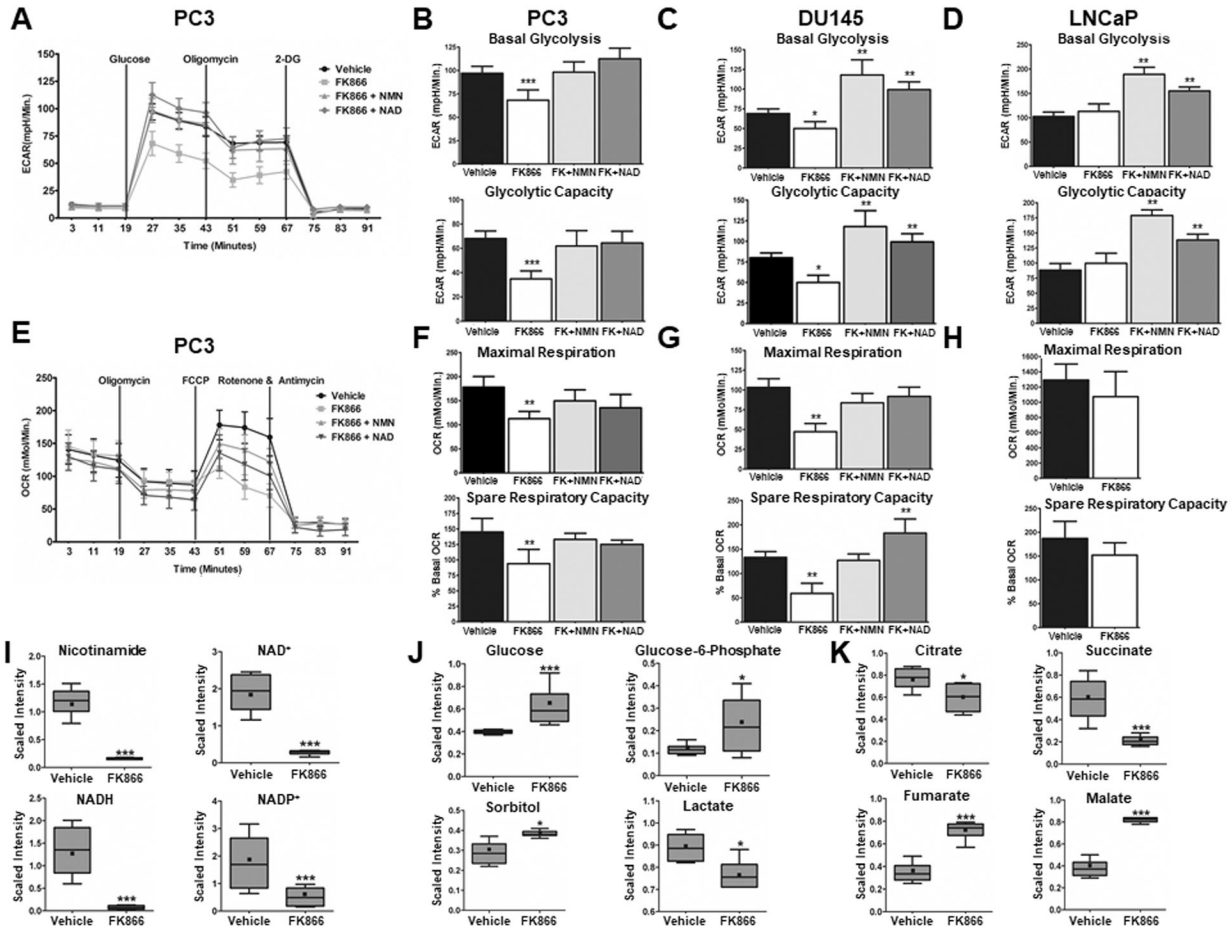

Figure 5: Pharmacological inhibition of NAMPT reduces glycolytic and mitochondrial capacity.

A, Representative trace of a glycolytic stress test in PC3 cells following treatment with FK866 (100nM) for 24Hrs in the absence or presence of exogenous NMN (500μM) or NAD^+ (100μM) (N = 3). B-D, Quantification of basal glycolysis and glycolytic capacity in DU145, PC3, and LNCaP cells (N = 3). E, Representative trace mitochondrial stress test in PC3 cells following treatment with FK866 (100nM) for 24Hrs in the absence or presence of exogenous NMN (500μM) or NAD^+ (100μM) (N = 3). F-H, Quantification of basal respiration, maximal respiration, and spare respiratory capacity in PC3, DU145, and LNCaP cells (N = 3). I–K, Scaled intensity of nicotinamide containing metabolites (I), glycolytic metabolites (J), and TCA cycle metabolites (K) following treatment of PC3 cells with FK866 (100nM) for 24Hrs. (*p ≤ 0.05, **p ≤ 0.01, ***p ≤ 0.001)

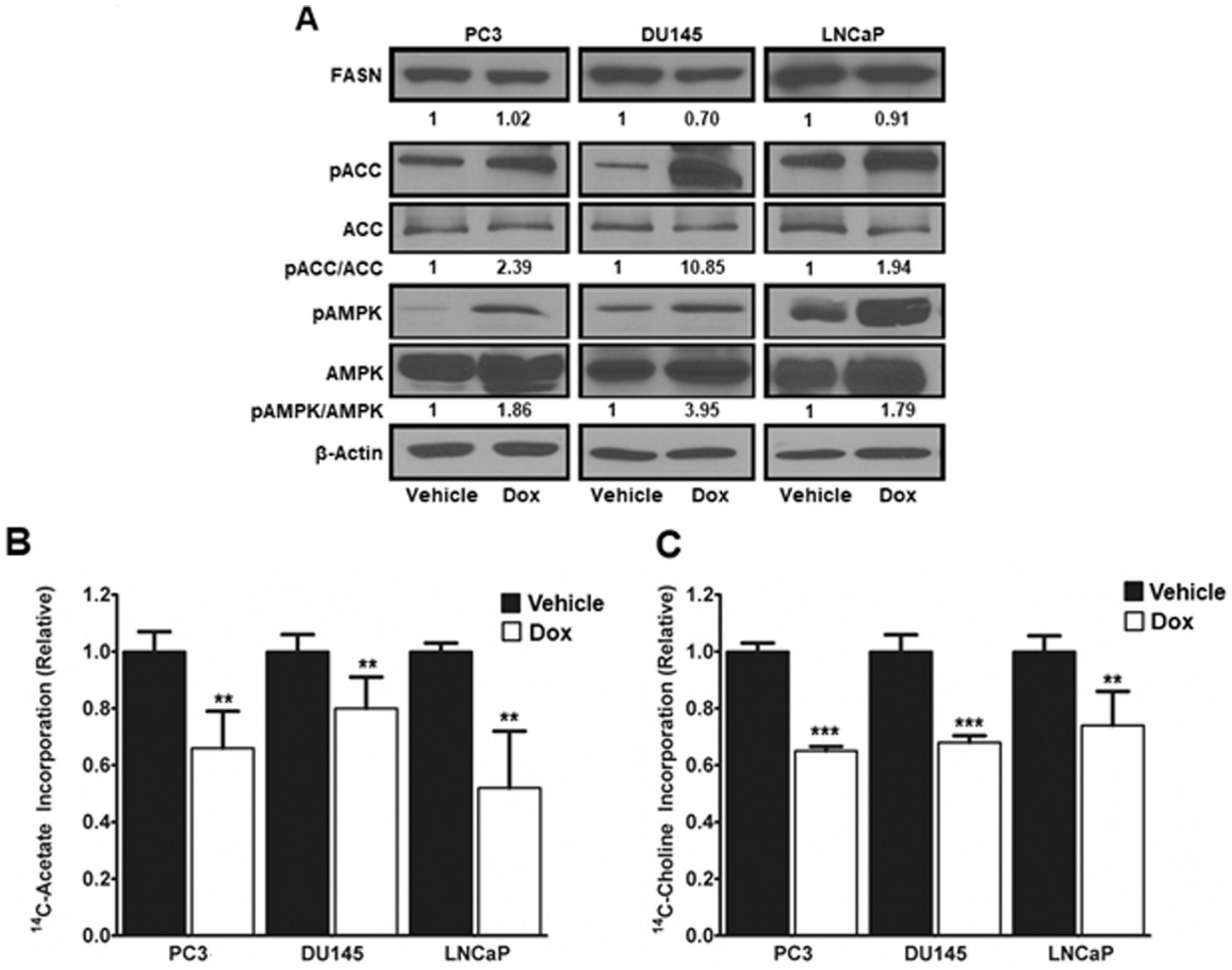

Figure 6: Expression of CD38 activates AMPK and inhibits fatty acid and lipid synthesis.

A, FASN, phospho-ACC, ACC, phospho-AMPK, AMPK, and β-Actin levels determined by western blot in PC3, DU145, and LNCaP cells following induction of CD38 by doxycycline (1μg/ml). Phospho-to-total ratios were determined by densitometry of single bands using β-Actin as a loading control. B, Fatty acid synthesis in PC3, DU145, and LNCaP cells as determined by incorporation of ^{14}C-acetate into lipid following induction of CD38 for 96Hrs (N = 3). C, Lipid synthesis in PC3, DU145, and LNCaP cells as determined by incorporation of ^{14}C-choline into lipid following induction of CD38 for 96Hrs (N = 3). (*$p \leq 0.05$, **$p \leq 0.01$, ***$p \leq 0.001$)

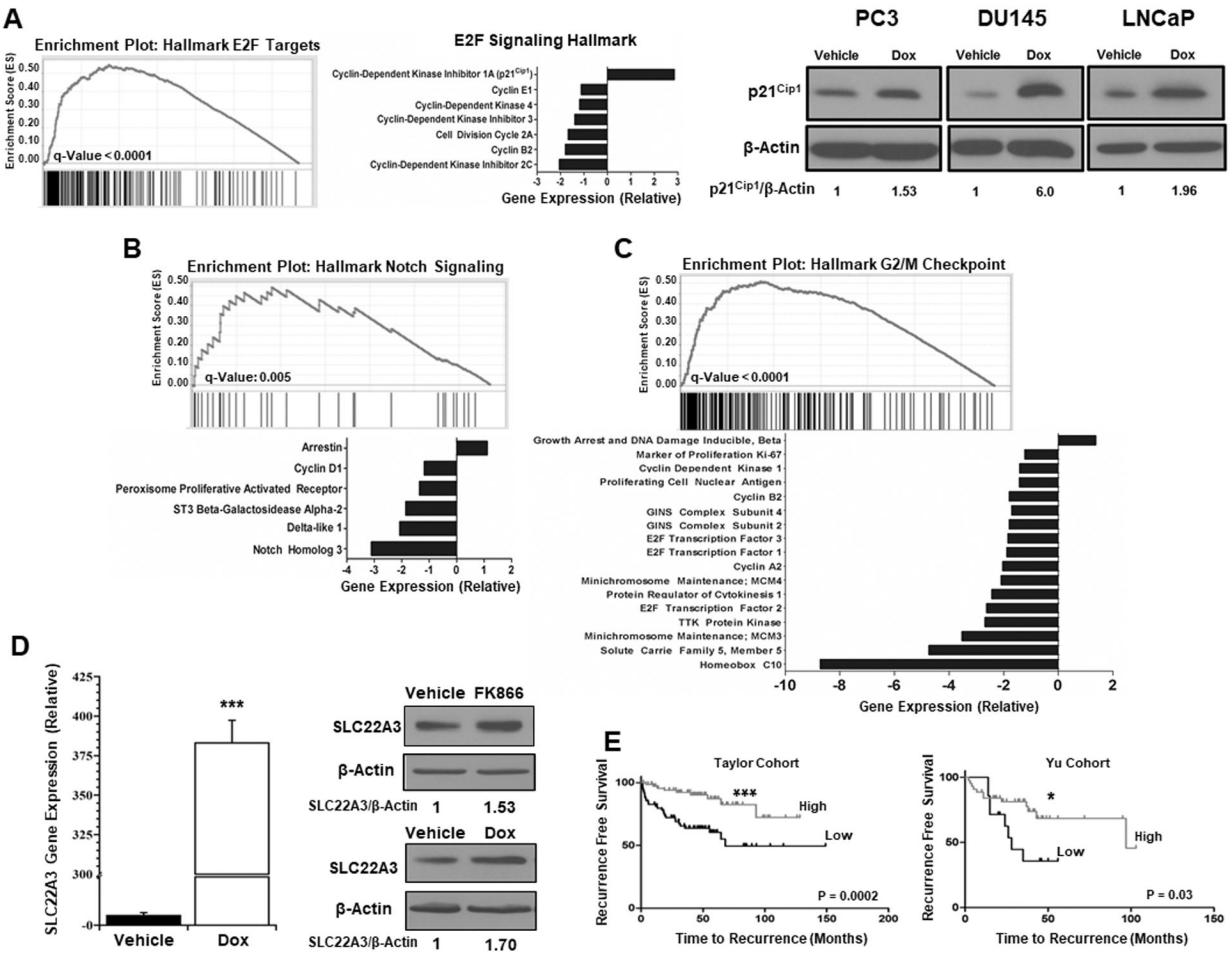

Figure 7: CD38 reprograms the transcriptome of PCa cells.

A, Gene set enrichment plot of genes altered by CD38 also included in an established E2F target hallmark signature (M5925). The bar graph represents gene expression values for a subset of genes contained in the E2F hallmark gene list. Expression of the cell cycle inhibitor $p21^{Cip1}$ was determined by western blotting following treatment with Doxycycline (1μg/ml) for 96Hrs with β-Actin as a loading control. B, Gene set enrichment plot of the genes affected by CD38 within a hallmark NOTCH signaling gene set (M5903). The bar graph represents relative expression levels of a subset of genes within the NOTCH signaling hallmark indicative of a non-proliferative phenotype. C, Gene set enrichment plot of genes affected by CD38 that exhibit a similar expression pattern to genes contained within the hallmark G2M checkpoint (M6901). The bar graph represents relative expression of genes contained within the G2M checkpoint hallmark consistent with a non-proliferative phenotype. D, *SLC22A3* expression in LNCaP cells following induction of CD38. Expression of SLC22A3 in LNCaP cells determined by western blot following treatment with FK866 (100nM) for 24Hrs or doxycycline (1μg/ml) for 96Hrs, respectively. E, Recurrence free survival as a function of SLC22A3 in the Taylor and Yu cohorts (27,28). (*$p \leq 0.05$, **$p \leq 0.01$, ***$p \leq 0.001$)

Table 1:
CD38 does not alter metabolic pathway gene expression.

Metabolic pathway gene expression as a function of CD38. Fold changes are expressed relative to vehicle control −/+ standard deviation (N=5).

Pathway	Gene Symbol	Gene Name	Fold	Change		Padj
Glycolysis	HK1	hexokinase 1	1.59	−/+	0.12	0.0000
	HK2	hexokinase 2	1.26	−/+	0.04	0.0000
	GCK	glucokinase (hexokinase 4)	1.14	−/+	0.55	0.6570
	GPI	glucose-6-phosphate isomerase	1.03	−/+	0.06	0.1792
	GAPDH	glyceraldehyde-3-phosphate dehydrogenase	-1.02	−/+	0.07	0.5036
	GLYCTK	glycerate kinase	-1.16	−/+	0.07	0.0043
	ENO1	enolase 1, (alpha)	-1.09	−/+	0.05	0.0000
	PKM	pyruvate kinase, muscle	-1.48	−/+	0.05	0.0000
	LDHA	lactate dehydrogenase A	1.14	−/+	0.05	0.0000
	LDHB	lactate dehydrogenase B	1.14	−/+	0.06	0.0000
Tricarboxylic Acid Cycle	PDK1	pyruvate dehydrogenase kinase, isozyme 1	1.49	−/+	0.04	0.0000
	CS	citrate synthase	1.18	−/+	0.07	0.0000
	ACO1	aconitase 1, soluble	-1.27	−/+	0.05	0.0000
	ACO2	aconitase 2, mitochondrial	1.50	−/+	0.10	0.0000
	IDH1	isocitrate dehydrogenase 1 (NADP+), soluble	1.50	−/+	0.09	0.0000
	IDH2	isocitrate dehydrogenase 2 (NADP+), mitochondrial	-1.29	−/+	0.06	0.0000
	OGDH	oxoglutarate (alpha-ketoglutarate) dehydrogenase	-1.14	−/+	0.11	0.0000
	MDH1	malate dehydrogenase 1, NAD (soluble)	1.14	−/+	0.05	0.0000
	MDH2	malate dehydrogenase 2, NAD (mitochondrial)	1.11	−/+	-	0.0000
	PC	pyruvate carboxylase	1.04	−/+	0.06	0.1195
Fatty Acid Synthesis	ACLY	ATP citrate lyase	1.11	−/+	0.06	0.0000
	ACACA	acetyl-CoA carboxylase; alpha	-1.17	−/+	0.04	0.3451
	ACACB	acetyl-CoA carboxylase; beta	1.24	−/+	0.15	0.0000
	FASN	fatty acid synthase	-1.92	−/+	0.03	0.0000
NADH Dehydrogenase (Complex 1)	NDUFA1	NADH dehydrogenase (ubiquinone) 1; α subcomplex 1	1.22	−/+	0.12	0.0000
	NDUFA5	NADH dehydrogenase (ubiquinone) 1; α subcomplex 5	1.04	−/+	0.04	0.1617
	NDUFA6	NADH dehydrogenase (ubiquinone) 1; α subcomplex 6	1.35	−/+	0.07	0.0000
	NDUFA7	NADH dehydrogenase (ubiquinone) 1; α subcomplex 7	1.12	−/+	0.07	0.0000
	NDUFA9	NADH dehydrogenase (ubiquinone) 1; α subcomplex 9	1.31	−/+	0.09	0.0000
	NDUFA12	NADH dehydrogenase (ubiquinone) 1; α subcomplex 12	1.18	−/+	0.09	0.0000
Succinate Dehydrogenase (Complex II)	SDHA	succinate dehydrogenase complex (subunit A)	1.28	−/+	0.08	0.0000
	SDHB	succinate dehydrogenase complex (subunit B)	1.22	−/+	0.07	0.0000
	SDHC	succinate dehydrogenase complex (subunit C)	-1.11	−/+	0.07	0.0008

Pathway	Gene Symbol	Gene Name	Fold	Change		Padj
	SDHD	succinate dehydrogenase complex (subunit D)	1.09	−/+	0.04	0.0003
Cytochrome C Red u etas e (Complex III)	UQCRB	ubiquinol-cytochrome c reductase; binding protein	1.22	−/+	0.09	0.0000
	UQCRC1	ubiquinol-cytochrome c reductase; core protein I	1.01	−/+	0.09	0.7548
	UQCRC2	ubiquinol-cytochrome c reductase; core protein II	1.19	−/+	0.06	0.0000
	UQCR10	ubiquinol-cytochrome c reductase; complex III (subunit X)	1.47	−/+	0.11	0.0000
	UQCR11	ubiquinol-cytochrome c reductase; complex III (subunit XI)	1.09	−/+	0.09	0.0000
Cytochrome C Oxidase (Complex IV)	COX10	COX10 heme A:farnesyltransferase cytochrome c oxidase assembly factor	1.10	−/+	0.08	0.0071
	COX14	C0X14 cytochrome c oxidase assembly factor	1.15	−/+	0.11	0.0000
ATP Synth as e (F_o Complex)	ATP5F1	ATP synthase; mitochondrial Fo complex (subunit B1)	1.13	−/+	0.07	0.0000
	ATP5S	ATP synthase; mitochondrial Fo complex (subunit S)	-1.06	−/+	0.08	0.0989
	ATP5I	ATP synthase; mitochondrial Fo complex (subunit E)	1.01	−/+	0.09	0.6758
	ATP5L	ATP synthase; mitochondrial Fo complex (subunit G)	1.19	−/+	0.09	0.0000
ATP Synth as e (F_1 Complex)	ATPAF1	ATP synthase mitochondrial F1 complex; assembly factor 1	1.08	−/+	0.06	0.0000
	ATPAF2	ATP synthase mitochondrial F1 complex; assembly factor 2	-1.03	−/+	0.08	0.3633